Synthesis and characterization of phosphate doped $BaPr_{1-y}(Y/Yb/Tm)_yO_{3-\delta}$

P. J. Keenan, A. D. Smith, P.R. Slater*

School of Chemistry, University of Birmingham, Birmingham. B15 2TT. UK

*Correspondence to Prof. P.R. Slater
p.r.slater@bham.ac.uk

Abstract

In this paper we examine the effects of doping phosphate into yttrium, ytterbium, and thulium doped $BaPrO_3$. Through phosphate doping it is possible to achieve high levels of Y/Yb/Tm, and we show that it is possible to completely replace all the Pr with this co-doping strategy, albeit such phases contained small impurities. The samples were analysed through a combination of X-ray diffraction, TGA, Raman spectroscopy and conductivity measurements. Conductivity data indicated that these heavily Y/Yb/Tm doped samples, however, showed lower conductivities than reported for previously for low levels (10-20%) of Y/Yb doping.

Introduction

Materials with the perovskite structure have attracted significant interest in the fuel cell area for both electrolyte and electrode materials. For electrolyte materials, a range of perovskite systems have been investigated displaying high oxide ion conductivity and/or proton conductivity [1-3]. In terms of proton conducting perovskite electrolytes, systems containing large A site cations having a low electronegativity (Ba/Sr) and a tetravalent B site cation (Zr^{4+}/Ce^{4+}) have been investigated. Such systems, when doped with trivalent rare earth cations, have displayed high proton conductivities in humid atmospheres, as a

result of water incorporation into the oxide ion vacancies introduced on doping. Another perovskite system that has attracted considerable interest from the research community is rare earth doped $BaPrO_3$. This material was initially proposed as a proton conducting electrolyte by Fukui et al. [4] Subsequent work indicated that the conductivity in this system was p-type rather than proton conductivity [5]. Furthermore issues have been raised regarding the instability of $BaPrO_3$ in CO_2 containing environments [6,7]. A range of further studies have been performed on this system, examining the effect of different rare earth dopants on the conductivity and cell symmetry [5, 8-10].

All these prior studies have focused on low levels of rare earth (Ln) dopants, i.e. $BaPr_{1-x}Ln_xO_{3-y}$ ($x \leq 0.2$). In this work we examine the possibility to increase the doping level through co-doping with phosphate, with a view to reducing the Pr content, and hence the electronic contribution to the conductivity. This approach stems from our prior work on oxyanion (MO_4^{n-}; M = Si, P, S) doping of $Ba_2(In/Sc)_2O_5$ and $BaCe_{1-x}(Y/Yb)_xO_{3-y}$ to synthesise new proton conducting perovskites. Using this strategy the Si, P and S reside on the B cation octahedral site in perovskites but with the oxide ions filling 4 of the available 6 oxide ion positions around the site. This doping strategy has been shown to enhance the oxide ion conductivity in perovskite systems containing high levels of oxide ion vacancies, e.g. $Ba_2(In/Sc)_2O_5$, through the introduction of disorder onto the oxygen sublattice, with proton conductivity observed in wet atmospheres due to water incorporation into the remaining vacant sites surrounding. In addition to this oxyanion doping has been shown to enhance the CO_2 stability of the doped $Ba_2(In/Sc)_2O_5$ systems, which is attributed to the introduction of these acidic dopants reducing the basicity of the system [11-14]. These oxyanion dopants have also been shown to be able to be accommodated into a range of

other perovskites, both electrolyte and electrode systems, showing that the perovskite structure is amenable to their incorporation [15-23].

In this paper we therefore extend this work to the $BaPrO_3$ system with a view to using co-doping with phosphate to increase the acceptor dopant (Y^{3+}, Tb^{3+}, Tm^{3+}) level and so reduce the Pr content, with a view to trying to reduce the high electronic conductivity level and improve the CO_2 stability, and so reintroduce the possibility of using such systems as proton conducting electrolytes.

Experimental

High purity $BaCO_3$, Pr_6O_{11}, Y_2O_3, Yb_2O_3 Tm_2O_3 and $NH_4H_2PO_4$were used to prepare Praseodymium containing samples $BaPr_{0.25}(Y/Yb/Tm)_{0.5}P_{0.25}O_{3-y}$ and samples $Ba(Y/Yb/Tm)_{0.75}P_{0.25}O_{3-y}$. A small (5%) excess of $BaCO_3$ was employed, in order to overcome Ba loss at elevated temperatures, and eliminate Ba deficient impurity phases (such as $Ba_3(Y/Yb/Tm)_4O_9$) as has been seen in other studies synthesising similar Ba containing phases [12,13]. For the samples without Pr ($Ba(Y/Yb/Tm)_{0.75}P_{0.25}O_{3-y}$), higher $BaCO_3$ excess (10%) was required to overcome Ba loss and hence limit the formation of Ba deficient impurities. In these particular cases, even with this higher level of Ba excess, such impurities could not be completely eliminated. In each case, the powders were intimately ground and heated initially to 1000°C for 12 hours. They were then ball-milled (350 rpm for 1 hour, Fritsch Pulverisette 7 Planetary Mill) and reheated to 1300°C for 12-24 hours (with intermediate regrind). The resulting powders were then ball-milled (350 rpm for 1 hour, Fritsch Pulverisette 7 Planetary Mill) a second time and pressed as pellets (1.3 cm diameter) and sintered at 1500°C for 4 hours. The pellets were covered in sample powder and the crucible was covered with a lid to limit the amount of Ba loss during the

sintering process. Powder X-ray diffraction (Bruker D8 diffractometer with Cu $K\alpha_1$ radiation) was used to demonstrate phase purity as well as for preliminary structure determination. For the latter, the GSAS suite of programs was used [24].

Raman spectroscopy measurements were made in order to provide evidence for the successful incorporation of phosphate. These measurements utilised a Renishaw inVia Raman microscope with excitation using a Cobolt Samba CW 532 nm DPSS Laser.

Given the presence of impurities in the $Ba(Y/Yb/Tm)_{0.75}P_{0.25}O_{3-y}$ samples, conductivity measurements were only performed on the single phase $BaPr_{0.25}(Y/Yb/Tm)_{0.5}P_{0.25}O_{3-\delta}$ samples. The sintered pellets (80-87% theoretical) were coated on each side with Pt paste and Pt electrodes were attached, and then heated to 850°C in air for 1 hour to ensure bonding to the pellet. Conductivities were then measured by AC impedance measurements (PSM 1735 N4L interface impedance analyser) in the range from 1Hz to 13 MHz. Measurements were made in dry N_2/O_2 and wet N_2/O_2 (in which the gas was bubbled at room temperature through water) to identify any protonic contribution to the conductivity and to determine if there was a p-type electronic contribution to the conductivity. The impedance spectra typically showed a single broad semicircle, corresponding to overlapping of bulk and grain boundary components, and so it was not possible to accurately extract individual bulk and grain boundary contributions. The total resistance was determined by the high intercept of this semicircle based on nonlinear least square fitting software Z-view [25].

The water contents of hydrated samples were determined from thermogravimetric analysis (Netzsch STA 449 F1 Jupiter Thermal Analyser). Samples were heated at 10°C min^{-1} to 1200°C in N_2, and the water content was determined from the observed mass loss.

The CO_2 stability of samples was determined using thermogravimetric analysis (Netzsch STA 449 F1 Jupiter Thermal Analyser). Samples were heated at 10 °C min^{-1} to 1000 °C in 1:1 CO_2 and N_2 mixture to determine at what temperature CO_2 pick up occurred.

Results and discussion

In order to synthesise $BaPr_{1-x}(Y/Yb/Tm)_xO_{3-y}$ samples with high levels (≥50%) of Y/Yb/Tm dopants, high levels (25%) of phosphate co-doping was required. Without such phosphate co-doping, high levels of $Ba_3(Y/Yb/Tm)_4O_9$ resulted showing the importance of phosphate doping in stabilising these high Y/Yb/Tm levels. With this approach, we were therefore able to successfully synthesise single phase samples of $BaPr_{0.25}Y_{0.5}P_{0.25}O_{3-y}$, $BaPr_{0.25}Yb_{0.5}P_{0.25}O_{3-y}$ and $BaPr_{0.25}Tm_{0.5}P_{0.25}O_{3-y}$ (figure 1a). Attempts were also made to prepare the endmember phases without Pr, i.e. $Ba(Y/Yb/Tm)_{0.75}P_{0.25}O_{2.75}$. While the formation of a perovskite phase was observed, it has so far not been possible to prepare these particular samples without the presence of small impurities (figure 1b). While addition of further excess Ba reduced the impurity levels, it was not possible to completely eliminate them, even by increasing the initial phosphate content. Consequently conductivity, hydration and CO_2 stability measurements were restricted to the single phase $BaPr_{0.25}(Y/Yb/Tm)_{0.5}P_{0.25}O_{3-y}$ samples.

From the X-ray diffraction data shown in figure 1a and b, the cell parameters for the $BaPr_{0.25}(Y/Yb/Tm)_{0.5}P_{0.25}O_{3-y}$ and $Ba(Y/Yb/Tm)_{0.75}P_{0.25}O_{2.75}$ phases were determined (tables 1 and 2). While the parent $BaPrO_3$ phase and systems doped with lower levels of rare earths (<20%) have been previously shown to be orthorhombic, at these higher dopant levels, the samples reported here appear cubic. The cell parameter data show a gradual

increase in cell volume on changing the dopant from Yb^{3+} to Tm^{3+} to Y^{3+}, which can be related to the increase in the ionic radius of the dopant. Somewhat, surprisingly the cell volumes of the $Ba(Y/Yb/Tm)_{0.75}P_{0.25}O_{2.75}$ samples were smaller than the corresponding $BaPr_{0.25}(Y/Yb/Tm)_{0.5}P_{0.25}O_{3-y}$ samples. A similar reduction in cell volume was reported by Knee et al. on doping 10% Y into $BaPrO_3$ [5]. Such reduction in cell parameters contradicts what might be expected from consideration of ionic radii for the replacement of Pr^{4+} by $Y^{3+}/Yb^{3+}/Yb^{3+}$. This therefore might suggest that either there is a significant proportion of the Pr in the Pr^{3+} (rather than Pr^{4+}) oxidation state, or that there is a degree of substitution of Y/Yb/Tm on the Ba site, the latter which might account for some of the difficulties in preparing single phase $Ba(Y/Yb/Tm)_{0.75}P_{0.25}O_{2.75}$ samples. In this respect, further investigations are required to clarify these results.

Raman data were collected for all the synthesised compositions as well as undoped $BaPrO_3$. For $BaPrO_3$ and $BaPr_{0.25}(Y/Yb/Tm)_{0.5}P_{0.25}O_{3-y}$ bands at ~ 650 and 940 cm^{-1} were observed (figure 2). The broad peak at 650cm^{-1} can be attributed to the praseodymium/rare earth dopant oxygen bonds while the peak at 940cm^{-1} (absent from undoped $BaPrO_3$) correlates with the phosphate group, confirming the presence of phosphate in the samples. Since, theoretically there should be no Raman active modes for a perfectly cubic perovskite, with the exception of possible second-order effects, the appearance of these bands suggests that although the XRD data indicate that the average structure is cubic for $BaPr_{0.25}(Y/Yb/Tm)_{0.5}P_{0.25}O_{3-y}$, there must be significant local distortions away from cubic symmetry in the doped systems. For the $Ba(Y/Yb/Tm)_{0.75}P_{0.25}O_{2.75}$ samples, the Raman data only showed the presence of the phosphate peak (figure 2).

In order to determine the level of possible water incorporation into $BaPr_{0.25}(Y/Yb/Tm)_{0.5}P_{0.25}O_{3-y}$, samples were heated under wet N_2 to 800 °C, before slow cooling (0.4 °C min^{-1}) to room temperature. X-ray diffraction confirmed that there was no decomposition of the samples on hydration (figure 3). The water contents were then determined by a TGA measurement, with the results shown in table 3. Overall water contents between 0.09 and 0.17 moles per formula unit were observed, indicating significant water incorporation.

The conductivities of the $BaPr_{0.25}(Y/Yb/Tm)_{0.5}P_{0.25}O_{3-y}$ samples were then investigated under both dry and wet conditions in nitrogen and oxygen atmospheres. The conductivity data are shown in figures 4-6 respectively, with representative impedance data shown in figure 7. Comparing dry and wet N_2 conditions, all the $BaPr_{0.25}(Y/Yb/Tm)_{0.5}P_{0.25}O_{3-y}$ samples showed a small improvement in the wet N_2 atmospheres at lower temperatures, which suggests the presence of a protonic contribution, consistent with the observation of significant water incorporation. The total conductivities (table 4, 5) were, however, substantially lower than reported for undoped $BaPrO_3$ and 10-20% rare earth doped $BaPrO_3$ [5]. In terms of the measurements in O_2, very similar conductivities under dry and wet conditions were observed for $BaPr_{0.25}Yb_{0.5}P_{0.25}O_{3-y}$ and $BaPr_{0.25}Tm_{0.5}P_{0.25}O_{3-y}$, while $BaPr_{0.25}Y_{0.5}P_{0.25}O_{3-y}$ showed a small increase under wet O_2 conditions, which again may be indicative of proton conductivity. Comparing the conductivities under dry N_2 and dry O_2, the data for $BaPr_{0.25}Yb_{0.5}P_{0.25}O_{3-y}$ and $BaPr_{0.25}Tm_{0.5}P_{0.25}O_{3-y}$, show a slightly higher conductivity in dry O_2 over the entire temperature range, indicative of a p-type electronic conductivity as observed for undoped $BaPrO_3$ and 10-20% rare earth doped $BaPrO_3$. Overall the results, however, indicate that

these heavily doped $BaPr_{0.25}(Y/Yb/Tm)_{0.5}P_{0.25}O_{3-y}$ samples show poor conductivities. Thus, while the electronic conductivity appears to have been suppressed compared to prior studies, and there is some evidence in support of a protonic contribution to the conductivity, the values obtained are not sufficiently high for applications. In this respect, the high phosphate levels required to achieve single phase samples may lead to a large degree of vacancy trapping and so suppress the conductivity. Such defect trapping at high oxyanion levels was proposed in prior studies by our group of $Ba_2In_2O_5$ [26]. In fact, it is probably this ability of phosphate to accommodate and hence stabilise the oxide ion vacancies around it (due to the preference for tetrahedral rather than octahedral coordination) that allows for the accommodation of higher levels of acceptor dopants (Y/Yb/Tm) than are achievable normally.

While the conductivity data showed a significant reduction on (Y/Yb/Tm) and phosphate co-doping, the impact on the CO_2 stability was also investigated. Many doped perovskite proton conductors (such as $BaCeO_3$) show poor stability on heating in a CO_2 containing atmosphere at typical fuel cell operating temperatures (500 – 700 °C), with the observation of significant mass increases, starting at 550°C, due to the formation of $BaCO_3$ [27]. Therefore the stabilities of $BaPr_{0.25}(Y/Yb/Tm)_{0.5}P_{0.25}O_{3-y}$ in a CO_2 environment were examined. The TGA profiles on heating in 1:1 CO_2 and N_2 showed, however, that these compositions are also susceptible to partial decomposition in a CO_2 atmosphere, although the mass increase was seen at slightly higher temperatures compared to doped $BaCeO_3$, with a gradual increase at 600°C and a more rapid increase seen around 750 °C for both $BaPr_{0.25}Yb_{0.5}P_{0.25}O_{3-y}$ and $BaPr_{0.25}Tm_{0.5}P_{0.25}O_{3-y}$ (figure 8).

Conclusions

The data show that it is possible to dope large levels of Y/Yb/Tm into $BaPrO_3$ through co-doping with phosphate, most likely related to the stabilization of the high levels of oxide ion vacancies around the phosphate group (due to its preference for tetrahedral rather than octahedral coordination). The conductivity measurements showed, however, significantly lower values than for under $BaPrO_3$ or 10-20% rare earth doped $BaPrO_3$, although in the present systems, there was evidence for a protonic contribution in humid atmospheres**.** Overall, the results further highlight the ability of perovskites to accommodate oxyanion groups on the B site, but suggest that in terms of conducting properties, the level of such dopants should be kept low to prevent a high degree of oxygen vacancy trapping.

Acknowledgements

We would like to express thanks to the University of Birmingham (studentships for AS/PJK) for funding.

References

1. K. D. Kreuer, *Solid State Ion.*, 1997, **97**, 1-15.
2. T. Norby, *Solid State Ion.*, 1999, **125**, 1-11.
3. A. Orera and P. R. Slater, *Chem. Mat.*, 2010, **22**, 675-690.
4. T. Fukui, S. Ohara and S. Kawatsu, *J. Power Sources*, 1998, **71**, 164-168.
5. C. S. Knee, A. Magraso, T. Norby and R. I. Smith, *Journal of Materials Chemistry*, 2009, **19**, 3238-3247.
6. A. Magraso, X. Solans, J. T. S. Irvine and M. Segarra, *Ceramics International*, 2009, **35**, 1819-1827.
7. V. P. Gorelov, B. L. Kuzin, V. B. Balakireva, N. V. Sharova, G. K. Vdovin, S. M. Beresnev, Y. N. Kleshchev and V. P. Brusentsov, *Russ. J. Electrochem.*, 2001, **37**, 505-511.
8. A. Magraso, F. Espiell, M. Segarra and J. T. S. Irvine, *J. Power Sources*, 2007, **169**, 53-58.
9. L. P. Li, J. R. Wu, M. Knight and S. M. Haile, Electrochemical Society, 2002,**28,** 58-66
10. S. J. Stokes and M. S. Islam, *J. Mater. Chem.*, 2010, **20**, 6258-6264.
11. J. F. Shin, L. Hussey, A. Orera and P. R. Slater, *Chem. Commun.*, 2010, **46**, 4613-4615.

12. J. F. Shin, D. C. Apperley and P. R. Slater, *Chem. Mat.*, 2010, **22**, 5945-5948.
13. J. F. Shin, A. Orera, D. C. Apperley and P. R. Slater, *J. Mater. Chem.*, 2011, **21**, 874-879.
14. J. F. Shin and P. R. Slater, *J. Power Sources*, 2011, **196**, 8539-8543.
15. C. A. Hancock and P. R. Slater, *Dalton Trans.*, 2011, **40**, 5599-5603.
16. J. M. Porras-Vazquez, E. R. Losilla, P. J. Keenan, C. A. Hancock, T. F. Kemp, J. V. Hanna and P. R. Slater, *Dalton Trans.*, 2013, **42**, 5421-5429.
17. A. D. Smith, J. F. Shin and P. R. Slater, *J. Solid State Chem.*, 2013, **198**, 247-252.
18. J. M. Porras-Vazquez, T. F. Kemp, J. V. Hanna and P. R. Slater, *J. Mater. Chem.*, 2012, **22**, 8287-8293.
19. J. M. Porras-Vazquez, T. Pike, C. A. Hancock, J. F. Marco, F. J. Berry and P. R. Slater, *J. Mater. Chem. A*, 2013, **1**, 11834-11841.
20. J. C. Pérez-Flores, N. Nasani, D. Pérez-Coll, P. R. Slater and D. P. Fagg; J. Mater. Chem. A 4, 11069-11076, 2016.
21. L. dos Santos-Gómez, J. M. Porras-Vázquez, E. R. Losilla, D. Marrero-López, P. R. Slater; J. Alloys and Compounds 835, 155437, 2020.
22. A.D. Smith, M. James, P.R. Slater; ECS Transactions 91, 1425-1436, 2019
23. A. Jarvis, P.R. Slater; Crystals *7*(6), 169, 2017.
24. A. C. Larson and R. B. Von Dreele, Los Alomos National Laboratory, Los Alomos NM, Editon edn., 1994.
25. D. Johnson, *Scribner associates Inc*, 2007.
26. J. F. Shin, K. Joubel, D. C. Apperley and P. R. Slater, *Dalton Trans.*, 2012, **41**, 261-266.
27. M. J. Scholten, J. Schoonman, J. C. Vanmiltenburg and H. A. J. Oonk, *Solid State Ion.*, 1993, **61**, 83-91.

Table 1 Cell parameter data for $BaPr_{0.25}(Y/Yb/Tm)_{0.5}P_{0.25}O_{3-y}$ (cubic cell)

Sample (nominal composition)	cell Parameter a_0 (Å)	Unit cell volume (Å^3)
$BaPr_{0.25}Y_{0.5}P_{0.25}O_y$	4.307(1)	79.89(5)
$BaPr_{0.25}Yb_{0.5}P_{0.25}O_y$	4.283(1)	78.61(4)
$BaPr_{0.25}Tm_{0.5}P_{0.25}O_y$	4.2891(3)	78.90(1)

Table 2 Cell parameter data for $Ba(Y/Yb/Tm)_{0.75}P_{0.25}O_{2.75}$ (cubic cell)

Sample (nominal composition)	cell Parameter a_0 (Å)	Unit cell volume (Å^3)
$Ba_2Y_{1.5}P_{0.5}O_y$	4.2819(8)	78.50(4)
$Ba_2Yb_{1.5}P_{0.5}O_y$	4.2547(7)	77.02(4)
$Ba_2Tm_{1.5}P_{0.5}O_y$	4.2571(5)	77.15(3)

Table 3 Water contents for hydrated $BaPr_{0.25}(Y/Yb/Tm)_{0.5}P_{0.25}O_{3-y}$

Sample (nominal composition)	**Moles of water per formula unit**
$BaPr_{0.25}Y_{0.5}P_{0.25}O_{3-y}$	0.17(1)
$BaPr_{0.25}Yb_{0.5}P_{0.25}O_{3-y}$	0.09(1)
$BaPr_{0.25}Tm_{0.5}P_{0.25}O_{3-y}$	0.15(1)

Table 4 Total conductivity data for $BaPr_{0.25}(Y/Yb/Tm)_{0.5}P_{0.25}O_{3-y}$ in dry and wet N_2 atmospheres

Sample (nominal composition)	**Conductivity (S cm^{-1})**			
	500 °C		800 °C	
	Dry N_2	Wet N_2	Dry N_2	Wet N_2
$BaPr_{0.25}Y_{0.5}P_{0.25}O_{3-y}$	2.5×10^{-5}	5.9×10^{-5}	6.6×10^{-4}	8.1×10^{-4}
$BaPr_{0.25}Yb_{0.5}P_{0.25}O_{3-y}$	2.1×10^{-5}	2.7×10^{-5}	4.6×10^{-4}	$3.3. \times 10^{-4}$
$BaPr_{0.25}Tm_{0.5}P_{0.25}O_{3-y}$	9.8×10^{-6}	1.6×10^{-5}	3.8×10^{-4}	3.6×10^{-4}

Table 5. Total conductivity data for $BaPr_{0.25}(Y/Yb/Tm)_{0.5}P_{0.25}O_{3-y}$ in dry and wet O_2 atmospheres

Sample (nominal composition)	**Conductivity (S cm^{-1})**			
	500 °C		800 °C	
	Dry O_2	Wet O_2	Dry O_2	Wet O_2
$BaPr_{0.25}Y_{0.5}P_{0.25}O_{3-y}$	2.9×10^{-5}	3.6×10^{-5}	7.6×10^{-4}	8.7×10^{-4}
$BaPr_{0.25}Yb_{0.5}P_{0.25}O_{3-y}$	2.9×10^{-5}	2.6×10^{-5}	6.4×10^{-4}	6.2×10^{-4}
$BaPr_{0.25}Tm_{0.5}P_{0.25}O_{3-y}$	3.3×10^{-5}	3.2×10^{-5}	6.6×10^{-4}	6.5×10^{-4}

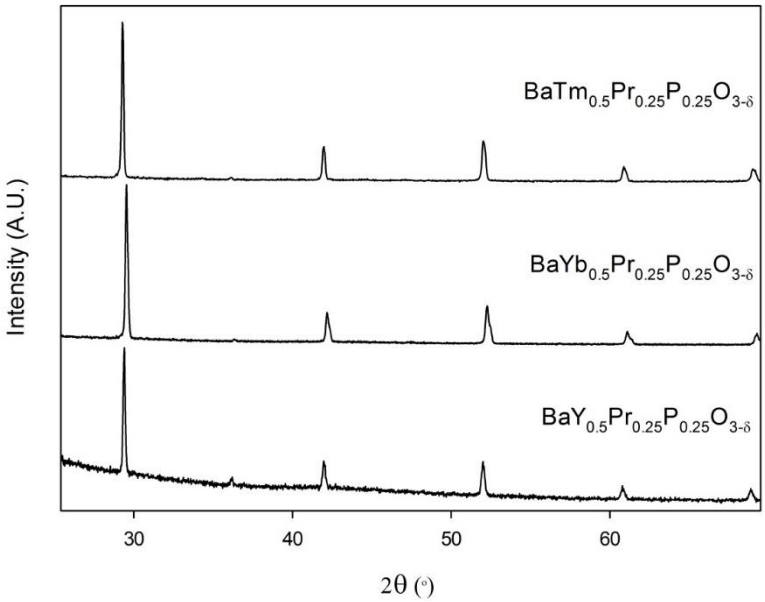

Fig1a. XRD patterns for $BaPr_{0.25}Y_{0.5}P_{0.25}O_{3-y}$, $BaPr_{0.25}Yb_{0.5}P_{0.25}O_{3-y}$ and $BaPr_{0.25}Tm_{0.5}P_{0.25}O_{3-y}$.

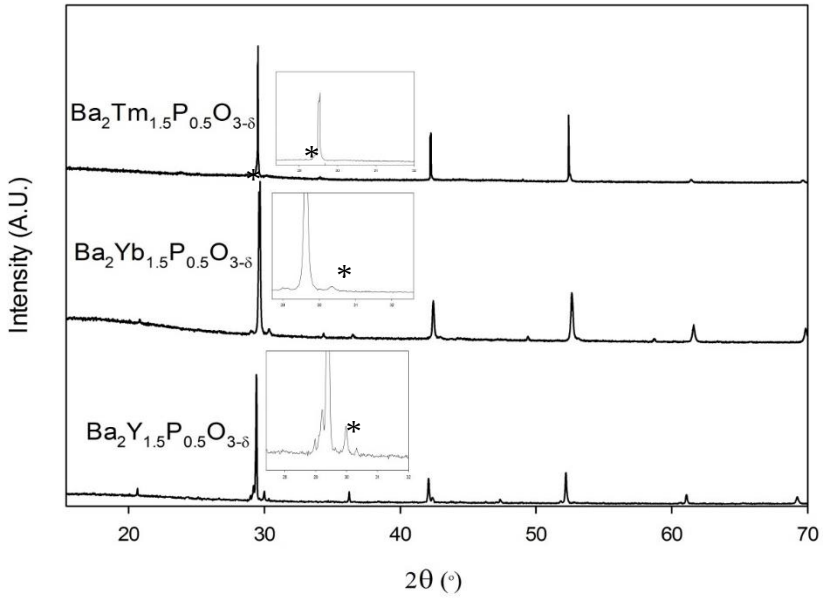

Fig1b XRD patterns for $BaY_{0.75}P_{0.25}O_{2.75}$, $BaYb_{0.75}P_{0.25}O_{2.75}$ and $BaTm_{0.75}P_{0.25}O_{2.75}$ (* =impurity phase)

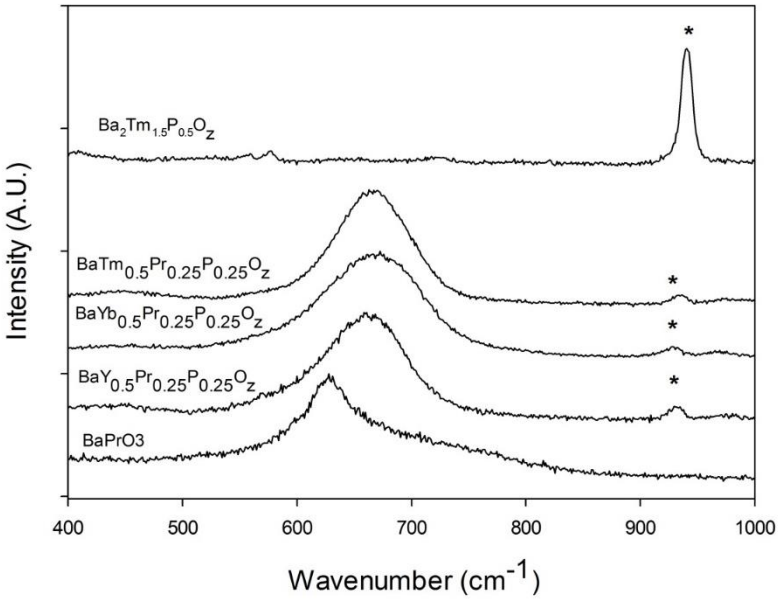

Fig 2. Raman spectra of $BaPrO_3$, $BaPr_{0.25}Y_{0.5}P_{0.25}O_{3-y}$, $BaPr_{0.25}Yb_{0.5}P_{0.25}O_{3-y}$, $BaPr_{0.25}Tm_{0.5}P_{0.25}O_{3-y}$ and $BaTm_{0.75}P_{0.25}O_{3-y}$ with peak showing the presence of phosphate indicated.

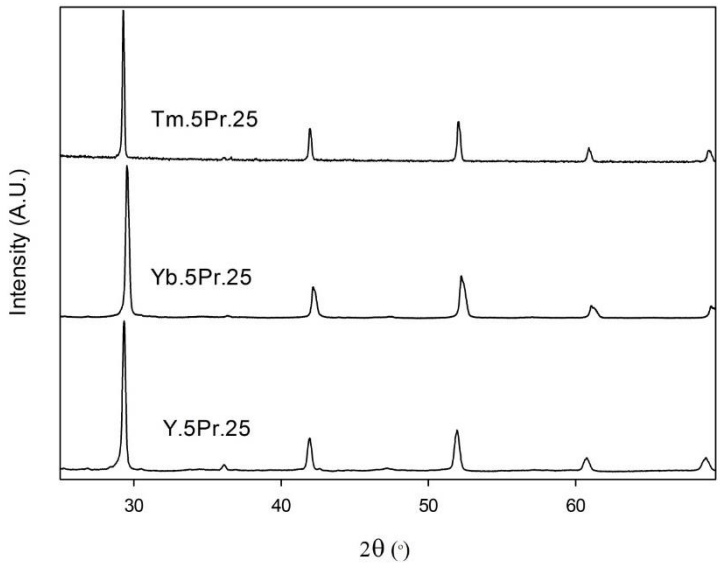

Fig 3. XRD patterns for hydrated $BaPr_{0.25}Y_{0.5}P_{0.25}O_{3-y}$, $BaPr_{0.25}Yb_{0.5}P_{0.25}O_{3-y}$ and $BaPr_{0.25}Tm_{0.5}P_{0.25}O_{3-y}$.

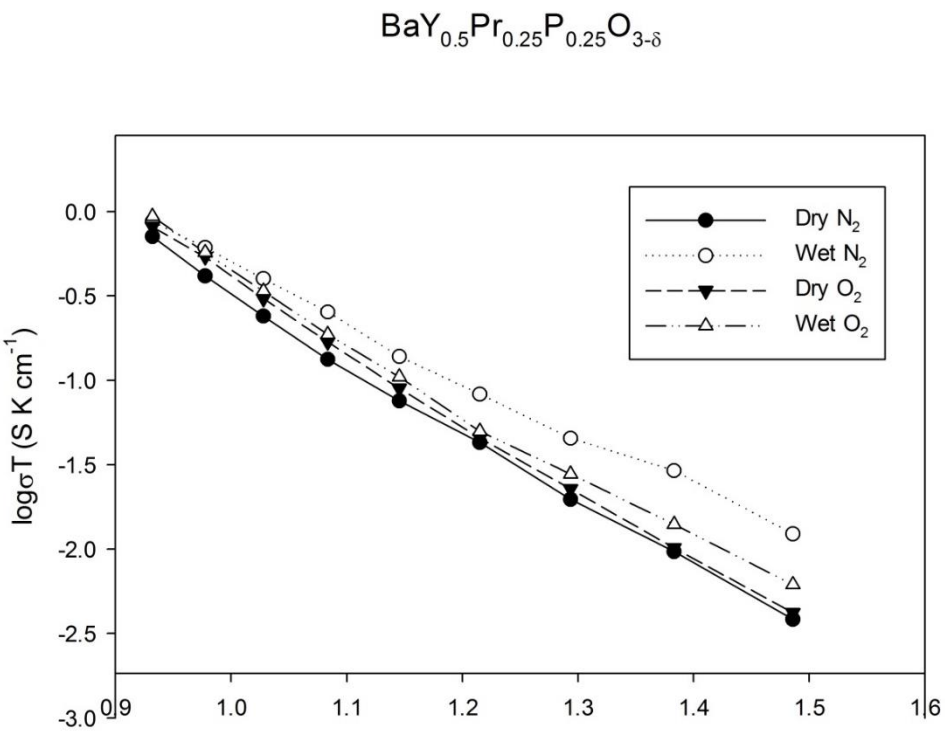

Fig. 4 Conductivity data for $BaPr_{0.25}Y_{0.5}P_{0.25}O_{3-y}$ in dry N_2 (black Circle), wet N_2 (white circle), dry O_2 (black triangle) and wet O_2 (white triangle).

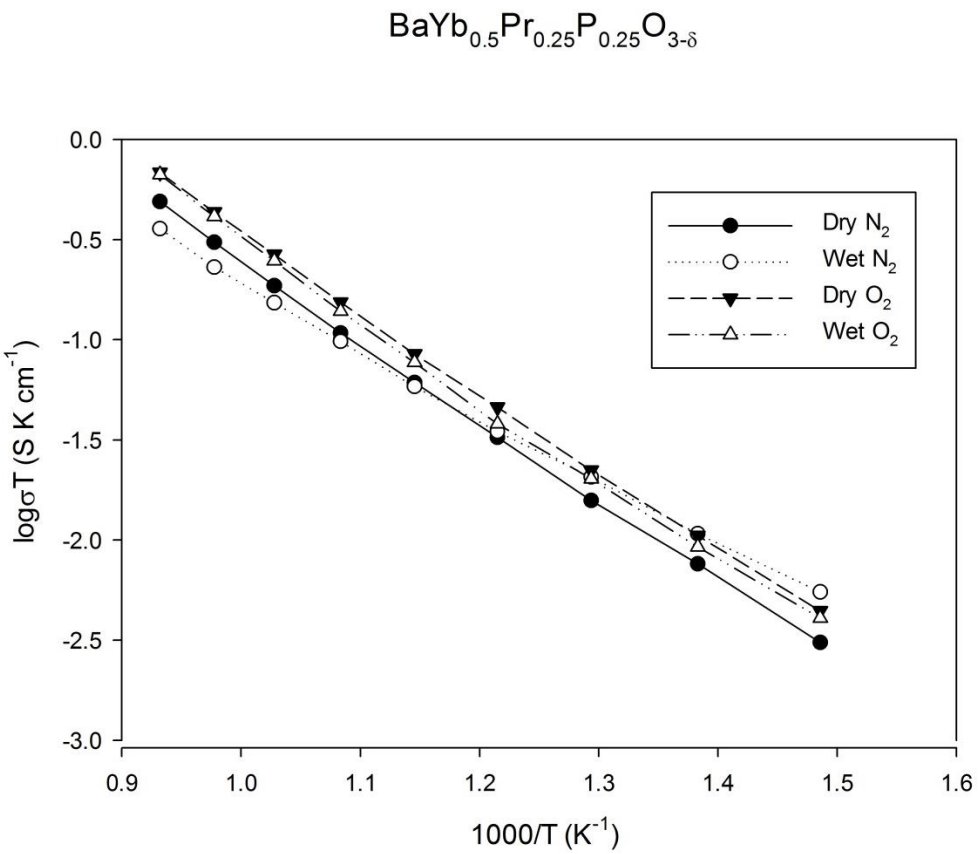

Fig. 5 Conductivity data for $BaPr_{0.25}Yb_{0.5}P_{0.25}O_{3-y}$.in dry N_2 (black Circle), wet N_2 (white circle), dry O_2 (black triangle) and wet O_2 (white triangle).

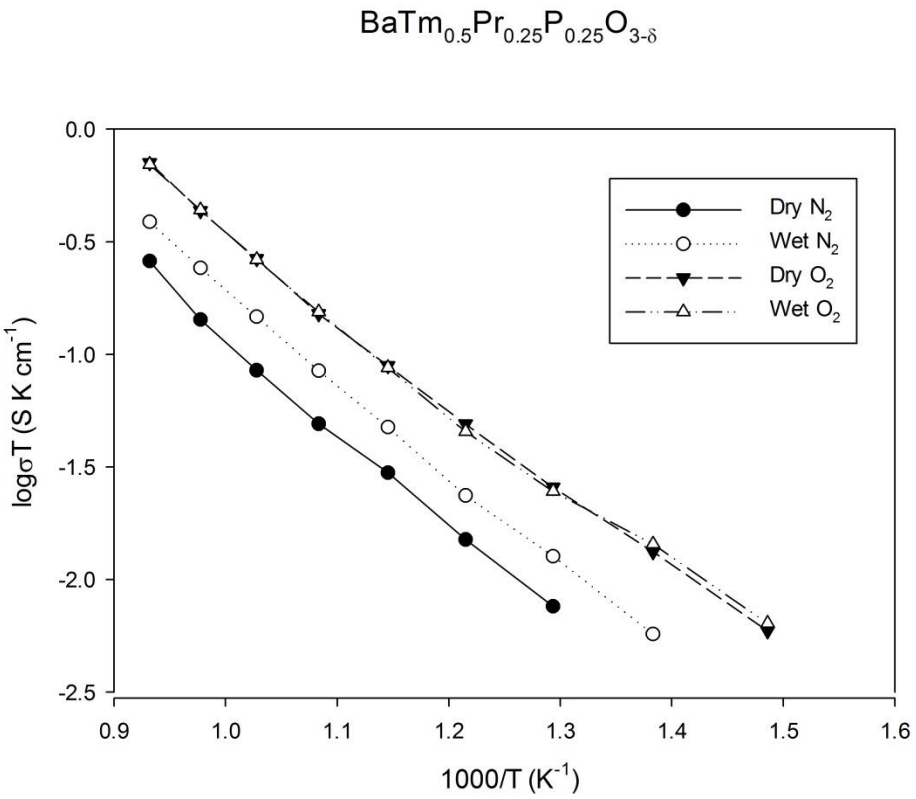

Fig. 6 Conductivity data for $BaPr_{0.25}Tm_{0.5}P_{0.25}O_{3-y}$ in dry N_2 (black Circle), wet N_2 (white circle), dry O_2 (black triangle) and wet O_2 (white triangle).

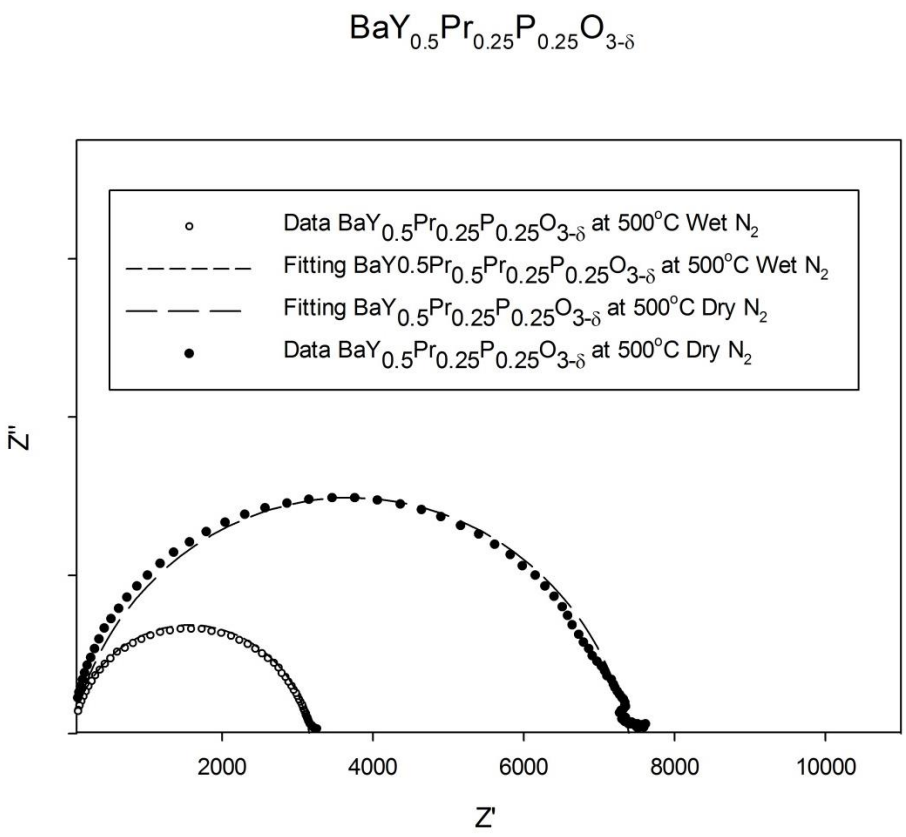

Fig 7 Impedance data for $BaPr_{0.25}Y_{0.5}P_{0.25}O_{3-y}$ at 500ºC in dry and wet N_2 atmosphere, showing the reduction in the resistance for the latter, indicative of a protonic contribution to the conductivity.

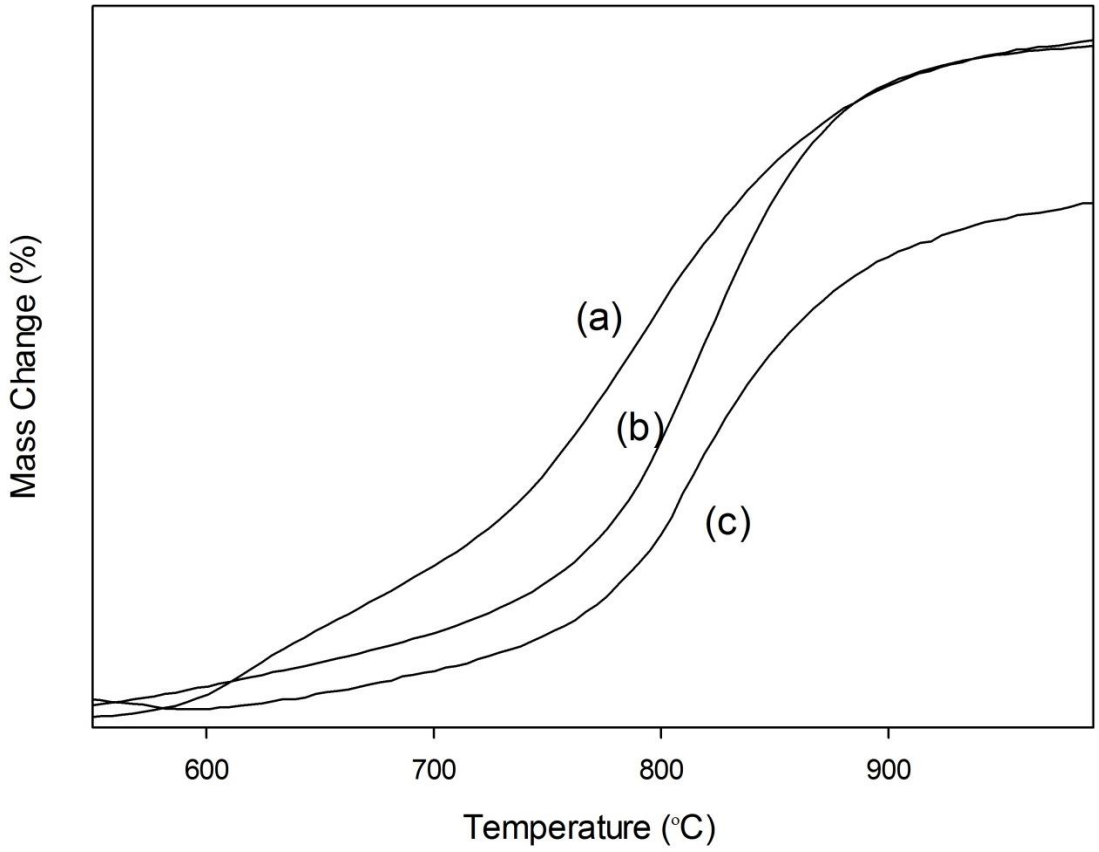

Fig. 8 TG profiles (10 °C min^{-1} to 1000 °C in 1:1 CO_2 and N_2 mixture) for (a) $BaPr_{0.25}Y_{0.5}P_{0.25}O_{3-y}$ (b) $BaPr_{0.25}Yb_{0.5}P_{0.25}O_{3-y}$ and (c) $BaPr_{0.25}Tm_{0.5}P_{0.25}O_{3-y}$.